

Reactive Landing Controller for Quadruped Robots

Francesco Roscia¹, Michele Focchi^{1,2}, Andrea Del Prete³, Darwin G. Caldwell⁴, and Claudio Semini¹

Abstract—Quadruped robots are machines intended for challenging and harsh environments. Despite the progress in locomotion strategy, safely recovering from unexpected falls or planned drops is still an open problem. It is further made more difficult when high horizontal velocities are involved. In this work, we propose an optimization-based reactive Landing Controller that uses only proprioceptive measures for torque-controlled quadruped robots that free-fall on a flat horizontal ground, knowing neither the distance to the landing surface nor the flight time. Based on an estimate of the Center of Mass horizontal velocity, the method uses the Variable Height Springy Inverted Pendulum model for continuously recomputing the feet position while the robot is falling. In this way, the quadruped is ready to attain a successful landing in all directions, even in the presence of significant horizontal velocities. The method is demonstrated to dramatically enlarge the region of horizontal velocities that can be dealt with by a naive approach that keeps the feet still during the airborne stage. To the best of our knowledge, this is the first time that a quadruped robot can successfully recover from falls with horizontal velocities up to 3 m/s in simulation. Experiments prove that the used platform, Go1, can successfully attain a stable standing configuration from falls with various horizontal velocity and different angular perturbations.

I. INTRODUCTION

LEGGED robots are designed to traverse rough terrains. Thanks to the progress of the last two decades, they have become lighter and stronger, enabling agile locomotion. Different types of gaits, such as trotting or crawling, have been investigated and successfully developed for quadrupedal robots. In contrast to advances in locomotion, relatively little research has been done on safely recovering after unexpected falls or planned drops. These abilities can be beneficial for both navigating harsh environments and preventing significant damage in case of involuntary falls.

Animals with righting reflexes have inspired many previous works on improving robotic landing capabilities, such as cats [1] and squirrels [2]. These works focus on dorso-ventrally reorienting the main body so that the limbs point toward the ground, e.g., mimicking cats with a flexible spine [3]. Some authors explored the inertial effects of flywheels, tails, and limbs for reorienting the robot when it falls. The work presented in [4] used a flywheel to control the tilt angle



Fig. 1. Based only on proprioceptive measures, during a fall the proposed Landing Controller (LC) adjusts the limbs posture in order to drive the robot to stable standing configuration after Touch Down (TD), avoiding bounces, feet slippage and undesirable contacts with the ground.

effectively; [5] proved that two flywheels with intersecting rotational axes can actuate both roll and pitch, allowing for non-planar jumps and landings. Many researchers have introduced a tail, which is an additional link that rotates about an axis that does not pass through the robot Center of Mass (CoM) [6]–[8]. However, a tail can only perform limited corrections due to its restricted range of motion and it adds weight and complexity to the robot. In [9] Mini Cheetah was provided with heavy boots to improve the influence on torso rotation. In that work, purely vertical falls with large rotations on the sagittal plane are handled by a combination of off-line optimization and supervised machine learning. The drawback of increasing the limbs' inertia is that the robot becomes tailored for the specific task of landing since planning problems can no longer rely on the assumption of mass-less legs. There is copious literature on approaches based on Trajectory Optimization (TO) to achieve movements in the air, such as jumps, spins, and flips. TO is used extensively for planning and controlling robots with a large number of Degrees of Freedom (DoFs). However, many of these approaches often neglect the landing phase and rely on the assumption of perfect tracking of the optimized trajectory to accomplish a safe landing. Minor errors in timing can complicate the execution of the landing task. In [10], flips were executed using the joint torques from the optimization as feed-forward commands, with Proportional Derivative (PD) joint feedback to track the optimized joint trajectories. However, tracking errors before the take-off affect the ballistic trajectory, resulting in poor landing configurations. The same issues are found in [11] and [12], which introduced a framework for performing highly dynamic 2D and 3D jumps with long flight times by combining off-line contact timings of Single Rigid Body Dynamics (SRBD), off-line whole-body TO, and high-frequency tracking controller. The MIT Mini Cheetah can perform a rich set of aerial movements, as shown in [13]. Motions are planned via centroidal momentum-based

The authors are with:

¹ Dynamic Legged Systems (DLS) lab, Istituto Italiano di Tecnologia (IIT), Genoa, Italy,

² Department of Information Engineering and Computer Science (DISI), University of Trento, Trento, Italy

³ Industrial Engineering Department (DII), University of Trento, Trento, Italy,

⁴ Advanced Robotics, Istituto Italiano di Tecnologia (IIT), Genoa, Italy.

Emails: {name.surname}@{iit, unitn}.it

The publication was created with the co-financing of the European Union FSE-REACT-EU, PON Research and Innovation 2014-2020 DM1062 / 2021.

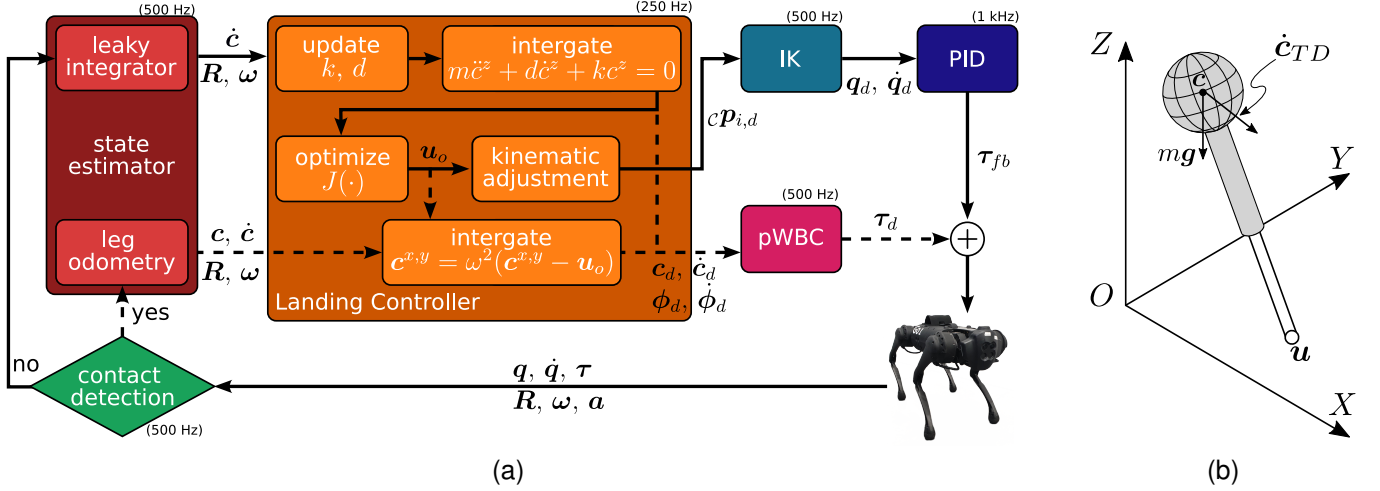


Fig. 2. (a) Overview of the landing controller framework. When the robot is in the flying phase, the virtual foot location is continuously re-optimized using the template model VHSIP, and the feet are shifted accordingly. Once landing is detected, the last computed trajectory for the CoM and trunk orientation is tracked. The dashed branches are active only after TD is detected. (b) The 3D VHSIP model used to describe the robot dynamics after TD.

nonlinear optimization and then tracked using a variational-based optimal controller [14]. Landing is accomplished using a simple joint PD controller stabilizing a fixed landing position. Therefore, only small heights are considered. Several works based on Reinforcement Learning (RL) and Model Predictive Control (MPC) present interesting landing strategies. Using a deep RL algorithm and sim-to-real transfer via domain randomization, [15] shows Spacebot performing consecutive 2D jumps in a micro-gravity environment. Even if the method is tailored to uneven terrains, tests are conducted on flat and rigid ground. A Vicon system provides measures for the robot's absolute position and orientation. How to extend the results to real-world 3D conditions with more dramatic impacts and inertial effects is unclear. [16] addresses the problem of landing on celestial bodies too. In particular, they propose a model-free RL controller with an auto-tuning reward function to address attitude and landing control on Near-Earth asteroids for which gravity cannot be supposed to be a central force. In [17], MIT Mini Cheetah is dropped from a CoM height of 1 m above the ground. The heuristics-guided MPC allows the robot to push onto the ground enough to arrest its downward momentum and return to a stable standing state within two steps. A recent work [18] implements heuristics to shift the feet posture for landing based on physical intuitions. However, the approach lacks feasibility guarantees grounded on a model of the system. In [19], a complete control framework can select optimal contact locations and timings in real-time. The controller consists of a Neural Network (NN) with two hidden layers providing warm-start trajectories for a nonlinear kino-dynamic TO (that employs a SRBD model), which is solved online in an MPC fashion. The robot safely recovers from drops of up to 8 m in simulation and up to 2 m in experiment starting with different orientations, but involving only vertical falls. The bottleneck of this framework is the NN: if a solution is not found within 300 ms, a new request is made and the optimization restarts. The framework works in real-time, and 300 ms represents an extensive interval of time for the flying phase of a fall: it corresponds to a height of about 0.5 m, starting with zero velocity. Therefore, falls from

reduced heights may not be addressed with this approach.

A. Proposed Approach

This paper addresses the problem of landing on a flat horizontal surface for a quadruped robot. Remarkably, the objective is to define a control strategy that satisfies the following requirements once the robot touches the ground:

- (R1) no bounces after landing;
- (R2) the trunk must not hit the ground;
- (R3) the feet must not slip;
- (R4) impact forces should be limited to avoid damaging the robot structure;
- (R5) the robot must reach a stable standing state.

To meet these requirements, we model the dynamics of the quadruped after the touch down as a Variable Height Springy Inverted Pendulum (VHSIP). The use of a spring model is not novel in the literature [20]–[22]. Despite its low complexity, the VHSIP template model captures the linear dynamics of the robot with sufficient accuracy and is inherently suitable for damping impacts with the terrain. A low-dimensional model allows us to design a control architecture with a short computation time, keeping it adequately reactive to change the control strategy at TD promptly. Our approach relies only on proprioceptive measurements, so no motion capture or visual perception system is required.

B. Contribution

The main contributions of this work are as follows.

- We introduce a real-time *omni-directional* Landing Controller (LC) framework (Fig. 2a), which can handle horizontal velocity, is tolerant to TD timing uncertainties, and does not require an estimate of the absolute robot position.
- We demonstrate successful landings in both a simulation environment and with real hardware from various heights and significant horizontal velocity, up to 3 m/s dropping the robot from a height of 1 m. To our best knowledge, this is the first time a quadruped robot can recover

from a fall with such horizontal velocity relying only on proprioceptive measures.

- We present a detailed analysis showing advantages and limitations of our LC. We show that it outperforms a naive approach that does not move the feet when the robot is falling. Moreover, although the template model neglects angular dynamics, our approach can tolerate drops starting with non-negligible orientations, e.g., with a roll between -40° and 30° , or pitch rate from $-440^\circ/s$ to $210^\circ/s$.

Even though the approach was developed and tested for four-legged robots, it is generic enough to be easily extended to robots with any number of legs.

C. Outline

The remainder of this manuscript is organized as follows. In Section II, we discuss our template model and formally state the landing problem. The structure of the landing framework is detailed in Section III, and the motion control in Section IV. Finally, we present implementation details and results in Section V and we summarize the discussion in Section VI.

II. MODELING AND PROBLEM FORMULATION

The fall of a legged robot can be decomposed in two phases: a flying phase, in which the robot is subjected only to gravity, and a landing phase, which begins when limbs (typically the feet) come into contact with the environment and generate Ground Reaction Forces (GRFs). The switching instant between the two phases is named Touch Down (TD). In this section, we derive the equations of motion of the VHSIP model that we use as a template to formalize and address the landing problem.

A. Derivation of the VHSIP Model

Let us introduce an inertial coordinate frame \mathcal{W} , with the Z -axis orthogonal to a flat ground and the XY -plane lying on the ground. In this frame, a free-falling robot can be seen as a single rigid body of mass $m \in \mathbb{R}^+$, lumped at its CoM $\mathbf{c} = [c^x \ c^y \ c^z]^T \in \mathbb{R}^3$, having inertia $\mathbf{I} \in \mathbb{R}^{3 \times 3}$. The balance of linear and angular momenta states that the linear dynamics is constrained to follow the ballistic trajectory while the angular momentum $\mathbf{L} \in \mathbb{R}^3$ is conserved:

$$m(\ddot{\mathbf{c}} + \mathbf{g}) = 0 \quad \dot{\mathbf{L}} = \frac{d}{dt}(\mathbf{I}\boldsymbol{\omega}) = 0 \quad (1)$$

being $\mathbf{g} \in \mathbb{R}^3$ the (constant) gravity acceleration vector and $\boldsymbol{\omega} \in \mathbb{R}^3$ the robot angular velocity. If the robot has n_c contact points, the balance of linear and angular momenta rewrites as:

$$m(\ddot{\mathbf{c}} + \mathbf{g}) = \sum_{i=1}^{n_c} \mathbf{f}_i \quad \dot{\mathbf{L}} = \sum_{i=1}^{n_c} (\mathbf{p}_i - \mathbf{c}) \times \mathbf{f}_i \quad (2)$$

where $\mathbf{p}_i \in \mathbb{R}^3$ is the position of the i -th contact point on which the environment exerts the force $\mathbf{f}_i \in \mathbb{R}^3$. Under the assumptions of horizontal ground ($p_i^z = 0, \forall i = 1, \dots, n_c$),

and negligible variation of the angular momentum ($\dot{\mathbf{L}} \approx 0$), we obtain the relationship (for further details, see [23])

$$\ddot{\mathbf{c}}^{x,y} = \omega^2 (\mathbf{c}^{x,y} - \mathbf{u}), \quad (3)$$

where $\mathbf{u} \in \mathbb{R}^2$ is the Center of Pressure (CoP), defined as

$$\mathbf{u} \triangleq \frac{\sum_{i=1}^{n_c} f_i^z \mathbf{p}_i^{x,y}}{\sum_{i=1}^{n_c} f_i^z}.$$

The dynamics in the horizontal directions of the CoM are decoupled, but they depend on the vertical motion through

$$\omega^2 \triangleq (g^z + \ddot{c}^z) / c^z.$$

Let us assume the CoP to be constant, i.e., a *virtual foot*. The vector $\vec{c}\mathbf{u}$ can change its length and rotate about \mathbf{u} due only to the gravity force $m\mathbf{g}$ and the initial CoM velocity (that for our problem corresponds to the TD velocity $\dot{\mathbf{c}}_{TD}^{x,y}$, see Fig. 2b). If the CoM height is constant, (3) simplifies to the well-known Linear Inverted Pendulum (LIP) model [24]. Nevertheless, such assumption is too restrictive. Indeed, to achieve a smooth landing and dissipate the impact energy effectively, it is convenient to enforce the vertical CoM dynamics after TD to behave as a Mass-Spring-Damper (MSD) system:

$$m\ddot{c}^z + d\dot{c}^z + k(c^z - l_0) = F^z, \quad (4)$$

in which l_0 is the spring rest position, and $k, d \in \mathbb{R}^+$ are the *virtual stiffness* and *virtual damping* coefficients, respectively. If the joint controller already implements a gravity compensation strategy, one may assume $F^z = 0$. In this way, the vertical CoM dynamics is an autonomous system, depending only on the state at TD: c_{TD}^z and \dot{c}_{TD}^z . We will refer to (3)–(4) as the VHSIP model. Since the CoM dynamics of the VHSIP in the two horizontal directions are equivalent and decoupled, in the following analysis we refer only to the motion along the X -axis, keeping in mind that the same arguments are valid also for the motion along the Y -axis.

The system is associated with a conserved quantity: the so-called Orbital Energy $E(c^x - u^x, \dot{c}^x)$ [25]:

$$E = \frac{1}{2} \dot{r}^x h^2(r^x) + g^z r^x f(r^x) - 3g^z \int_0^{r^x} f(\xi) \xi d\xi$$

with $r^x = c^x - u^x$, $c^z = f(r^x)$ is a twice-differentiable function¹, f' its derivative and $h(r^x) = f(r^x) - f'(r^x)r^x$. If the CoM is moving toward the virtual foot with $E > 0$, then orbital energy is sufficient to let the CoM to pass over \mathbf{u} and continue on its way. If $E < 0$, then the CoM will stop and reverse the direction of motion before getting over the virtual foot. If $E = 0$, then the CoM converges to rest above \mathbf{u} , [26]. Therefore, robot configurations in equilibrium can be reached by selecting \mathbf{u} so that at TD the following condition holds

$$E(c_{TD}^x - u^x, \dot{c}_{TD}^x) = 0. \quad (5)$$

¹The scalar function f maps horizontal displacements to heights. It exists as long as $c^x(t)$ is a bijective function of time. As a matter of fact, in this case $c^x(t)$ admits an inverse which would allow us to write $c^z(t)$ as a function of $c^x(t)$. The trajectory $c^x(t)$ is bijective if the virtual foot u^x is constant and $\omega^2(t) > 0$. The former clause is already taken as an assumption. The latter occurs whenever the CoM does not penetrate the ground ($c^z > 0$) and there is no pulling force from the ground ($\ddot{c}^z > -g^z$): this clause is already verified for the problem we are considering.

In the capturability framework, such u is named Capture Point (CP). Whereas for the LIP model it is possible to explicitly compute the CP from the above equation, for our VHSIP model this is not the case. In the following, we show how we overcome this complexity.

B. Landing Problem

Now, we can state the problem more formally.

Problem Statement. Consider a robot that is free falling on a flat horizontal ground with negligible angular velocity. Without knowing the distance between the robot and the ground, find (if any) the parameters for the template VHSIP model (i.e., the virtual stiffness k , virtual damping d and virtual foot location u), that fulfill the requirements (R1), (R2), (R3), (R4), and (R5). Then, compute the joint torques that realize the CoM motion obtained with the selected template model.

III. METHODOLOGY

In this paragraph, the structure of our LC is introduced and discussed. At any sampling instant, we suppose that the TD is about to occur and use the template VHSIP model to compute a new CoM reference trajectory for landing. In this way, we can avoid estimating the robot's absolute position when no contact is active. During the flying phase, the system has to prepare to dissipate the kinetic energy throughout the landing phase. The robot should adjust its limbs to be able to place the virtual foot u (i.e., the CoP) on the CP at TD. Notice that (3)–(4) are defined in an inertial frame, but our LC is designed to be independent of absolute position estimates. We circumvent this limitation by introducing the terrain frame \mathcal{T} . First, we denote the robot CoM frame with \mathcal{C} . It has the origin on the CoM, the X_C -axis along the forward direction of the main body and the Y_C -axis orthogonal to it, pointing towards the left side (see Fig. 3). The terrain frame is a horizontal frame [27], hence the $X_T Y_T$ -plane is orthogonal to gravity and X_T and X_C lie on the same plane. We will refer to the distance between O_T and O_C during the flying phase as l_0 , which is a user-modifiable parameter. In particular, we set l_0 to the robot height in home configuration. For a given control interval, the frame \mathcal{T} is fixed and can be employed to compute the new CoM reference trajectory. At the subsequent control interval, one of the following two alternative conditions will arise:

- TD is detected. Thus, the CoM reference will be tracked, stabilizing the system.
- TD is not detected. In this case, a *kinematic adjustment* (detailed in Section III-D) is performed, in order to keep the feet aligned with the landing surface, i.e. on the $X_T Y_T$ -plane. Then, a new terrain frame is set and the process repeats.

The benefits of continuous re-computation are two-fold: to make the robot reactive and to avoid the need of state estimation². Since all the quantities in the remainder of this section are expressed in the terrain frame, henceforth, we will omit the frame for the sake of readability.

²We still have to estimate the linear velocity, but the implementation described in Section III-F mitigates the influence of accelerometer biases.

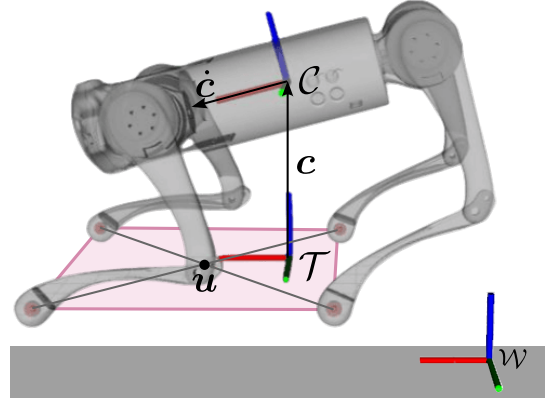


Fig. 3. The CoM frame \mathcal{C} has the origin located at the robot CoM and encapsulates the trunk orientation. The terrain frame \mathcal{T} is the horizontal reference frame for which the CoM has coordinates $c = [0 \ 0 \ l_0]^T$ when the robot is in air. After TD, \mathcal{T} is kept fix. Respectively, red, green and blue segments denote the X -, Y -, and Z -axis of the frames. The robot is shown performing the kinematic adjustment since its orientation is not horizontal and \dot{c} has a non-null horizontal component.

A. Vertical Motion Reference

In the context of the VHSIP model, the requirement (R1) is equivalent to having a critically-damped oscillator in (4), i.e., no oscillations in the height reference. Since k and d are tunable coefficients, this can be achieved setting the damping equal to $d = 2\sqrt{km}$ (critical damping). In this way, the two system poles are real and coincident in $\lambda = -\sqrt{k/m}$. The kinematic adjustment module guarantees that when the TD occurs, the CoM is always at distance l_0 from the floor. Then, the reference trajectory for the CoM in the vertical direction depends only on the TD velocity $\dot{c}_{TD}^z < 0$. The evolution of a critically-damped system can be computed in closed form:

$$\dot{c}^z(t) = e^{\lambda(t-t_{TD})} (\lambda(t-t_{TD}) + 1) \dot{c}_{TD}^z \quad (6a)$$

$$c^z(t) = e^{\lambda(t-t_{TD})} (t-t_{TD}) \dot{c}_{TD}^z + l_0 \quad (6b)$$

The stiffness k must be selected to ensure the minimum value for $c^z(t)$ is above the ground, preventing the contact between trunk and ground (requirement (R2)). Since the system is critically damped, this minimum is unique for $t > t_{TD}$. To find it, one can equate (6a) to zero and solve for t . The solution represents the time when maximum elongation occurs: $t_{\min} = t_{TD} - 1/\lambda$. Plugging t_{\min} into (6b), the minimum value of $c^z(t)$ is found:

$$c^z(t_{\min}) = -\frac{1}{\lambda} \frac{\dot{c}_{TD}^z}{e} + l_0$$

Therefore, letting Δ^z be the minimum terrain clearance, requiring that $c^z(t) \geq \Delta^z$ for $t \geq t_{TD}$ is equivalent to $c^z(t_{\min}) > \Delta^z$. This can be translated in a lower-bound for the stiffness coefficient using the definition of λ :

$$k \geq k_1 = \frac{m}{(e(\Delta^z - l_0))^2} (\dot{c}_{TD}^z)^2.$$

We set a maximum for the convergence time to prevent long dynamic evolution when TD velocity is low. Since (4) is a stable second-order system with coincident eigenvalues, it is at steady-state for $t \geq -7/\lambda$. Choosing the maximum time of convergence t_c , another limitation for the stiffness comes out:

$$k \leq k_2 = m(t_c/7)^2.$$

At every control instant, we fix the virtual stiffness to $k = \max\{k_1, k_2\}$ and update the virtual damping accordingly. Then, a new reference trajectory $c_d^z(t)$ is computed.

B. Horizontal Motion Reference

To prevent the robot from tipping over during landing and to drive it to a stable standing configuration (requirement **(R5)**), we seek for the (constant) virtual foot location u^x that drives the CoM above it with zero linear velocity when the system reaches steady-state, i.e. that attains zero orbital energy (5). Equation (3) can be rewritten in state-space form:

$$\underbrace{\begin{bmatrix} \dot{c}^x(t) \\ \ddot{c}^x(t) \end{bmatrix}}_{\dot{\mathbf{x}}(t)} = \underbrace{\begin{bmatrix} 0 & 1 \\ \omega^2(t) & 0 \end{bmatrix}}_{\mathbf{A}(t)} \underbrace{\begin{bmatrix} c^x(t) \\ \dot{c}^x(t) \end{bmatrix}}_{\mathbf{x}(t)} + \underbrace{\begin{bmatrix} 0 \\ -\omega^2(t) \end{bmatrix}}_{\mathbf{B}(t)} u^x \quad (7)$$

showing its nature of Linear Time Varying (LTV) system, with $\omega(t)$ evolving in time. Even if the dynamics is linear, its integration does not admit a closed-form solution because the matrix $\mathbf{A}(t)$ does not commute with its integral $\int_{t_{TD}}^t \mathbf{A}(\sigma) d\sigma$, [28]. To overcome this issue, we set up an Optimal Control Problem (OCP) to find the constant CoP position u^x that makes the CoM converge to it with null velocity over a finite horizon. Hereafter, when a time-varying variable appears with as subscript, e.g. k , it must be interpreted as evaluated at time kT_s , for instance $x_k = x(kT_s)$, being T_s the sampling time. Our OCP relies on forward Euler integration and it is formulated as

$$\begin{aligned} \min_{\mathbf{x}_k, u^x} \quad & w_p |\mathbf{C}_p \mathbf{x}_N - u^x|^2 + w_v |\mathbf{C}_v \mathbf{x}_N|^2 + w_u |u^x|^2 \\ \text{s.t.} \quad & \mathbf{x}_{k+1} = \bar{\mathbf{A}}_k \mathbf{x}_k + \bar{\mathbf{B}}_k u^x \quad k = 0, 1, \dots, N-1 \end{aligned} \quad (8)$$

having set $\bar{\mathbf{A}}_k = \mathbf{I}_{2 \times 2} + T_s \mathbf{A}_k$ and $\bar{\mathbf{B}}_k = T_s \mathbf{B}_k$. Above, $\mathbf{I}_{2 \times 2}$ the 2×2 identity matrix, and $\mathbf{C}_p = \begin{bmatrix} 1 & 0 \end{bmatrix}$ and $\mathbf{C}_v = \begin{bmatrix} 0 & 1 \end{bmatrix}$ are selection matrices that pick out position and velocity from the state \mathbf{x} , respectively. Moreover, $w_p, w_v, w_u \in \mathbb{R}^+$ are weights that penalize the final CoM deviation from the virtual foot u^x , the final CoM velocity, and the virtual foot distance from $O_{\mathcal{T}}$. The horizon N should be large enough to guarantee that at time NT_s the system is at steady-state. We solve (8) with a single shooting approach. For doing so, the knowledge of $\omega^2(t)$, $0 \leq t \leq NT_s$, is needed. Thus (4) must be forward integrated up to NT_s . Knowing $\omega^2(t)$ and recursively applying (3), we can express the state trajectory in terms of virtual foot and initial conditions. This results in an unconstrained Quadratic Program (QP) in the scalar optimization variable u^x :

$$\min_{u^x} J(\mathbf{x}_0, u^x) \triangleq \mathbf{x}_0^T \mathbf{Q}^x \mathbf{x}_0 + u^{xT} \mathbf{Q}^u u^x + 2\mathbf{x}_0^T \mathbf{Q}^{xu} u^x \quad (9)$$

\mathbf{Q}^x , \mathbf{Q}^u and \mathbf{Q}^{xu} are real matrices of dimensions 2×2 , 1×1 and 2×1 , respectively. For the sake of conciseness, we do not report their expression here. Zeroing the partial derivative of the cost $J(\cdot)$, the optimal virtual foot location is found:

$$u_o^x = \frac{\mathbf{Q}^{xuT}}{\mathbf{Q}^u} \mathbf{x}_0.$$

Notice that, because of the choice of the cost function, the minimization of $J(\cdot)$ corresponds to minimizing the Orbital

Energy. Repeating the same argument for the lateral component of the CoM, the coordinates of the virtual foot in the terrain frame are obtained. At this point, if a TD occurs, the robot must track the CoM reference trajectory. This is obtained by plugging \mathbf{u}_o into (3) and forward integrating along the horizon to get the horizontal components, while keeping the vertical component previously computed as described in (4). Conversely, if a TD does not occur, the kinematic adjustment introduced in Section III-D is performed, shifting the feet according to the optimal virtual foot location. Additionally, the terrain frame is updated and a new reference is computed.

C. Angular Motion Reference

Even though the VHSIP does not capture the angular dynamics of the robot, it is still valid within a limited range of orientations. Suppose the robot lands with a non-horizontal trunk. In that case, we plan the Euler angles $\phi_d \in \mathbb{R}^3$ to make the robot trunk reach a horizontal configuration while the second-order system in (4) attains the steady state. Euler rates can be used since the robot operates far enough from singular configurations: without any loss of generality, any representation of orientation could be adopted.

D. Kinematic Adjustment

During the flying phase, the robot limbs must prepare to realize the optimal CoP at TD. We call such motion *kinematic adjustment* [27]. Fig. 3 shows the robot while performing the kinematic adjustment. It consists in placing the robot feet \mathbf{p}_i on the vertices of a rectangle parallel to the landing surface, even if the robot trunk is not horizontal. The rectangle lies on the $X_{\mathcal{T}}Y_{\mathcal{T}}$ -plane and it is shifted such that its centroid is placed onto the optimal CoP \mathbf{u}_o : $\mathbf{p}_{i,d}(t) = \mathbf{p}_{i,0} + \alpha(t) \mathbf{u}_o$, where $\mathbf{p}_{i,0}$ is the position of the i -th foot when the robot is in the homing configuration. To avoid abrupt changes in the reference that would affect the orientation of the base, we perform a linear interpolation with $\alpha: t \rightarrow [0, 1]$. Denoting with ${}^c\mathbf{R}_{\mathcal{T}} \in SO(3)$ the rotation matrix describing the orientation of the terrain frame with respect to the trunk, we can express feet positions in the \mathcal{C} -frame

$${}^c\mathbf{p}_{i,d} = {}^c\mathbf{R}_{\mathcal{T}} \left(\mathbf{p}_{i,d} - \begin{bmatrix} 0 & 0 & l_0 \end{bmatrix}^T \right).$$

This motion of ${}^c\mathbf{p}_{i,d}$ can be realized with joint-space control. Desired joint configurations can be computed solving an Inverse Kinematic (IK) problem for each foot assuming mass-less legs: $\mathbf{q}_{i,d} = \text{IK}({}^c\mathbf{p}_{i,d})$, where $\mathbf{q}_{i,d}$ contains the desired angles of the joints on the i -th leg. The mechanical structure of our robot allows us to employ closed form IK at the position level and $\mathbf{q}_{i,d} \in \mathbb{R}^3$, $\forall i = 1, \dots, 4$. Desired joint velocities are computed considering the Cartesian-space error ${}^c\mathbf{e}_i = {}^c\mathbf{p}_{i,d} - {}^c\mathbf{p}_i$:

$$\dot{\mathbf{q}}_{i,d} = (\mathbf{J}_i(\mathbf{q}) + \varepsilon \mathbf{I}_{3 \times 3})^{-1} k_v {}^c\mathbf{e}_i$$

being $\mathbf{J}_i(\mathbf{q}_d) \in \mathbb{R}^{3 \times 3}$ the Jacobian matrix associated to the i -th foot, $\mathbf{I}_{3 \times 3}$ is the 3×3 identity matrix, $\varepsilon \in \mathbb{R}^+$ a regularization parameter, and $k_v \in \mathbb{R}^+$ a scaling factor. The joint trajectory is then tracked by means of a joint-space PD

feedback controller with diagonal positive-definite matrices of proportional and derivative gains \mathbf{K}_P^j and \mathbf{K}_D^j , and gravity compensation torque $\boldsymbol{\tau}_g(\mathbf{q})$:

$$\boldsymbol{\tau}_{fb} = \mathbf{K}_P^j(\mathbf{q}_d - \mathbf{q}) + \mathbf{K}_D^j(\dot{\mathbf{q}}_d - \dot{\mathbf{q}}) + \boldsymbol{\tau}_g(\mathbf{q}). \quad (10)$$

E. Touch Down Detection

We define the transition between the flying and landing phases, i.e., the Touch Down (TD), as the first time instant when all feet are in contact with the landing surface. Since torque estimations based on the motor current are available in our robotic platform, we identify the contact status of each foot based on an estimate of the Ground Reaction Forces (GRFs) exerted on it. Alternatively, mechanical switches or contact sensors could be employed, but these are typically expensive and sensitive devices that suffer from impacts. From torque measurements, we estimate the contact force $\hat{\mathbf{f}}_i$ exerted on the i -th foot as:

$$\hat{\mathbf{f}}_i = \mathbf{J}_i(\mathbf{q})^{-T} \mathbf{S}_i(\mathbf{c}(\mathbf{q}, \dot{\mathbf{q}}) + \mathbf{g}(\mathbf{q}) - \boldsymbol{\tau}) \quad (11)$$

where \mathbf{q} , $\dot{\mathbf{q}}$ and $\boldsymbol{\tau}$ are the measured joint positions, velocities and torques, respectively, \mathbf{c} is the centrifugal and Coriolis term, \mathbf{g} is the vector of gravitational effects, \mathbf{S}_i is the matrix that selects the torques associated to the i -th leg. According to the assumption of flat horizontal ground, a contact is detected if $\hat{f}_i^z \geq f_{th}^z$, with f_{th}^z a (small) robot-dependent threshold.

F. State Estimation

Because of the definition of the terrain frame and of the kinematic adjustment performed in the flying phase, we do not need to estimate the position of the CoM at TD: we can assume it to be $\mathbf{c}_{TD} = [0 \ 0 \ l_0]^T$. Our robot is equipped with an Inertial Measurement Unit (IMU) that outputs rotation matrix ${}_{\mathcal{W}}\mathbf{R}_{\mathcal{C}}$, angular velocity ${}_{\mathcal{C}}\boldsymbol{\omega}$ and linear acceleration ${}_{\mathcal{C}}\mathbf{a}$ (referred to the robot base frame). The linear acceleration in the inertial frame is retrieved considering the accelerometer bias ${}_{\mathcal{C}}\mathbf{b} \in \mathbb{R}^3$ as: $\mathbf{a} = {}_{\mathcal{W}}\mathbf{R}_{\mathcal{C}}({}_{\mathcal{C}}\mathbf{a} - {}_{\mathcal{C}}\mathbf{b}) - \mathbf{g}$. During the flying phase, we reconstruct the base linear velocity $\mathbf{v} \in \mathbb{R}^3$ making use of a leaky integrator, equally to [29]:

$$\hat{\mathbf{v}}_{k+1} = (\mathbf{I}_{3 \times 3} - \boldsymbol{\Gamma} T_s) \hat{\mathbf{v}}_k + \mathbf{I}_{3 \times 3} T_s \mathbf{a}_k \quad (12)$$

where $\boldsymbol{\Gamma} = \text{diag}(\gamma^x, \gamma^y, \gamma^z)$ is a diagonal matrix of positive discount factors in the three directions. Since the flying phase has a short time duration, the leaky integrator achieves satisfactory performances in mitigating the drift due to inaccuracies of bias estimation. The estimate $\hat{\mathbf{v}}_k$ is plugged into the robot full model for computing the CoM velocity during the flying phase. Conversely, we rely on leg odometry after TD to estimate the CoM position and velocity, as in [30].

IV. MOTION CONTROL DURING LANDING PHASE

In this section, we discuss the projection-based Whole Body Control (pWBC) we employ to track the computed CoM trajectory during the landing phase. First, we design a Cartesian impedance, attached at the CoM, to track the CoM reference after TD, stabilize the orientation, and reject disturbances on both linear and angular directions. The control law will generate a wrench $\mathbf{w}_d \in \mathbb{R}^6$ that we map into desired GRFs $\mathbf{f}_{i,d} \in \mathbb{R}^3$, at the robot's feet [30].

1) *Feedback Wrench*: A PD feedback term is computed to track the CoM reference and the base orientation:

$$\begin{aligned} \mathbf{w}_{fb}^{lin} &= \mathbf{K}_P^{lin}(\mathbf{c}_d - \mathbf{c}) + \mathbf{K}_D^{lin}(\dot{\mathbf{c}}_d - \dot{\mathbf{c}}), \\ \mathbf{w}_{fb}^{ang} &= \mathbf{K}_P^{ang} \mathbf{e}({}_{\mathcal{W}}\mathbf{R}_{\mathcal{C},d} {}_{\mathcal{W}}\mathbf{R}_{\mathcal{C}}^T) + \mathbf{K}_D^{ang}(\dot{\phi}_d - \dot{\phi}) \end{aligned}$$

where ${}_{\mathcal{W}}\mathbf{R}_{\mathcal{C},d}$ is the rotation matrix associated to the desired Euler angles ϕ_d and $\mathbf{e}: SO(3) \rightarrow \mathbb{R}^3$ is the mapping from a rotation matrix to the associated rotation vector.

2) *Feed-forward Wrench*: We annihilate the effects of the gravity force on the CoM through the feed-forward component

$$\mathbf{w}_g = [m\mathbf{g}^T \ \mathbf{0}_{3 \times 1}]^T.$$

To improve the tracking of a time-varying reference, the desired accelerations enter the controller with an additional feed-forward term

$$\mathbf{w}_{ff}^{lin} = m\ddot{\mathbf{c}}_d, \quad \mathbf{w}_{ff}^{ang} = {}_{\mathcal{T}}\mathbf{R}_{\mathcal{C}} \mathcal{I}_{\mathcal{C}} {}_{\mathcal{C}}\mathbf{R}_{\mathcal{T}} \dot{\boldsymbol{\omega}}_d,$$

where $\dot{\boldsymbol{\omega}}_d$ is deduced from the desired Euler angles and rates.

3) *Whole Body Controller*: After TD, the robot has all the feet in contact with the ground and the desired wrench

$$\mathbf{w}_d = \begin{bmatrix} \mathbf{w}_d^{lin} \\ \mathbf{w}_d^{ang} \end{bmatrix} = \mathbf{w}_{fb} + \mathbf{w}_g + \mathbf{w}_{ff}$$

is mapped to the stack of desired GRFs $\mathbf{f}_d \in \mathbb{R}^{3n_c}$ with

$$\mathbf{f}_d = \begin{bmatrix} \cdots & \mathbf{I}_{3 \times 3} & \cdots \\ & [\mathbf{p}_i - \mathbf{c}]_{\times} & \end{bmatrix}^{\dagger} \mathbf{w}_d \quad (13)$$

where $[\cdot]_{\times}$ is the skew-symmetric operator associated to the vector product and $[\cdot]^{\dagger}$ is the Moore-Penrose pseudo-inverse. The desired torque to be exerted by the joints of the i -th leg is $\boldsymbol{\tau}_{d,i} = \mathbf{c}_i(\mathbf{q}, \dot{\mathbf{q}}) - \mathbf{J}_i(\mathbf{q}) \mathbf{f}_{d,i}$.

V. RESULTS

A. Implementation details

The robot we use to demonstrate the validity of our approach is the torque-controlled quadruped Unitree Go1 Edu [31]. To visualize, simulate and interact with the robot, we developed and open-sourced Locosim [32], a platform-independent software framework designed for fast code prototyping. We implement both the pWBC and the LC in a Python ROS node, which relies on Pinocchio [33] for the computation of robot kinematics and dynamics and closes the loop at 500 Hz. The firmware of Go1 allows external inputs via the user datagram protocol (UDP) through an Ethernet connection. For computational efficiency, we implemented the calculation of the complete evolution of the VHSIP reference dynamics in C++, for which we provided Python bindings. The VHSIP dynamics is computed with a frequency of 250 Hz and linearly interpolated to match the controller frequency of

TABLE I
USER-MODIFIABLE PARAMETERS

Parameter	Meaning	Value
l_0	Nominal robot height	0.27 m
Δ^z	Minimum ground- c^z distance	0.10 m
t_c	Maximum settling time	1.2 s
f_{th}^z	Normal force threshold	18 N
$\gamma^x, \gamma^y, \gamma^z$	Leaky integrator discount factors	0.21 Hz

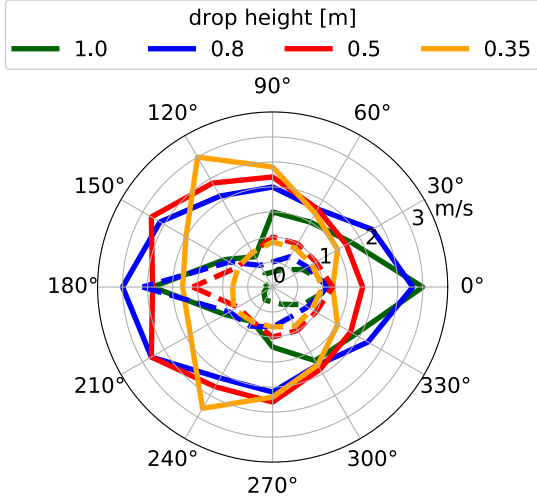


Fig. 4. Simulation results: polar plot of the maximum magnitude of the horizontal velocity vs. its orientation with respect to X_T -axis. Solid lines express the limits for our LC and dashed lines for the naive approach. 0° means that the $\dot{c}_{TD}^{x,y}$ is aligned with X_T and points toward the same direction, 180° means that it points in the opposite direction, and so on.

500 Hz. Since Python is not real-time compliant, monitoring the actual control loop frequency in simulation is essential before running the code with the real hardware. Nevertheless, we did not experiment delays that hampered the stability of our control framework. A list of user-modifiable parameters is reported in Table I.

B. Limits on the Horizontal Velocity

To emphasize the advantages of the proposed LC, we first compared it in simulation with a naive controller that keeps the feet at a constant position on the $X_T Y_T$ -plane during the flying phase and tracks c_d^z after TD. Here, we consider a landing task *achieved* only if the feet make contact with the ground and the robot reaches a standing still configuration (i.e., velocities below a threshold). Our goal is to show that the modulation of the virtual foot u_o is crucial to achieve a successful landing. Fig. 4 shows the range of TD horizontal velocities that can be handled using either our LC or the naive controller. For all the tested dropping heights, the LC can handle larger initial horizontal velocities in all the directions. The asymmetry of the polytopic regions results from the asymmetric mass distribution and joint limits.

C. Angular perturbations

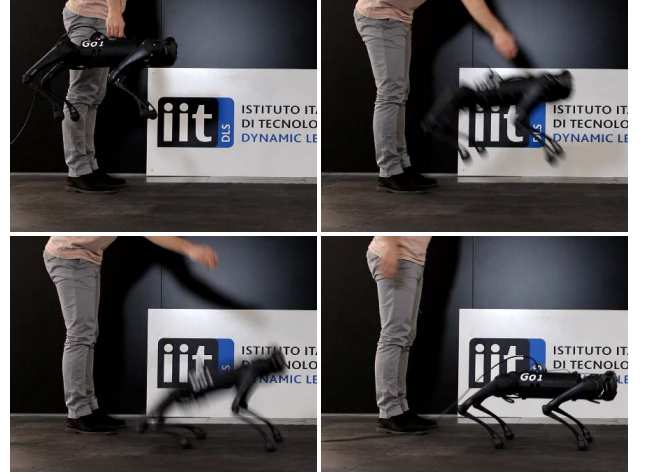
Here, we want to evaluate how tolerant our method is to angular perturbations, despite the fact that our template model does not describe the angular motion (see Section III-C). In simulation, we tested the robustness of our LC with respect to non-zero initial angular velocity and non-horizontal orientation of the trunk. We drop the robot from a height of 0.60 m (about 2.5 times its standing height) with a forward velocity of 1.0 m/s and we vary, one at the time, the initial values of roll and pitch angles and rates. The limit values for which our LC is able to achieve the landing task are in Table II.

D. Experiments

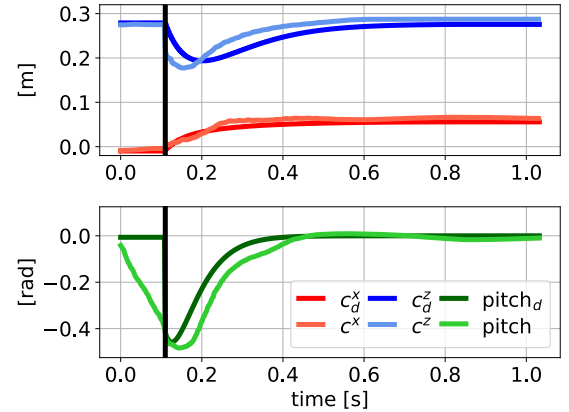
We have performed an extensive experimental study to

TABLE II
LIMITS OF ANGULAR PERTURBATIONS DROPPING GO1 FROM 0.6 m HEIGHT AND 1.0 m/s FORWARD VELOCITY

	min	max
roll angle $[\circ]$	-40	30
pitch angle $[\circ]$	-40	10
roll rate $[\circ/s]$	-380	390
pitch rate $[\circ/s]$	-440	210



(a)



(b)

Fig. 5. (a) Snapshots showing the experiment in which the robot is dropped from about 0.8 m in the forward direction with horizontal velocity of approx 1.0 m/s. (b) Desired and actual value for CoM position and pitch expressed in T -frame. The black vertical line represents the TD detection.

assess the performance of our LC. We used the 12 kg Go1 quadruped robot and dropped it from various heights and with different manually induced horizontal velocities in all the directions (forward, backwards, lateral left, lateral right). Fig. 5 illustrates a drop from about 0.8 m with non-zero horizontal velocity in the forward direction, as well as time plots of the reference and actual values of CoM position and robot orientation. The experiments proved that our LC can achieve successful landings using only proprioceptive measures, without knowing the absolute position of the robot when it falls. Other tests are reported in the accompanying video <https://youtu.be/KnmNbkhOKWI>.

VI. CONCLUSIONS

In this work, we presented a reactive model-based approach

for quadruped robot landing after unexpected falls or planned drops. A successful landing involves dissipating all the kinetic energy at the impact, bringing the robot to a complete stop while maintaining the feet in contact, without hitting the ground with the trunk. Tracking an impedance model turned out to be a suitable candidate to dissipate the excess of kinetic energy avoiding rebounds. The approach is reactive enough (500 Hz) to cope with lower heights than 0.5 m as in [19] and makes use only of proprioceptive measurements, being therefore independent of an external motion capture system. Furthermore, it is able to achieve *omni-directional* landing with significant horizontal velocity, up to 3.0 m/s. Our landing controller was extensively bench-marked in simulation and demonstrated to dramatically outperform a naive landing strategy that tracks the vertical impedance but does not adjust the feet locations according to the touch-down velocity. Despite employing a simplified model that relies upon a horizontal orientation assumption, the approach was demonstrated to tolerate a large range of orientation errors. An extensive experimental evaluation of omni-directional landing on the real robot Go1 was also presented, randomly dropping the robot in different ways.

Future research directions could improve the model descriptiveness, relaxing the assumption of negligible variation of the angular momentum, extending the region of feasible horizontal velocities and tolerable angular perturbations. Additionally, we want to extend the approach for landing onto non-horizontal surfaces.

REFERENCES

- [1] T. R. Kane and M. Scher, "A dynamical explanation of the falling cat phenomenon," *International journal of solids and structures*, vol. 5, no. 7, pp. 663–670, 1969.
- [2] N. H. Hunt, J. Jinn, L. F. Jacobs, and R. J. Full, "Acrobatic squirrels learn to leap and land on tree branches without falling," *Science*, vol. 373, no. 6555, pp. 697–700, 2021.
- [3] B. Shields, W. S. Robertson, N. Redmond, R. Jobson, R. Visser, Z. Prime, and B. Cazzolato, "Falling cat robot lands on its feet," in *Proceedings of the Australasian Conference on Robotics and Automation*, 2013, pp. 74–82.
- [4] H. Kolvenbach, E. Hampp, P. Barton, R. Zenkl, and M. Hutter, "Towards jumping locomotion for quadruped robots on the moon," in *2019 IEEE/RSJ International Conference on Intelligent Robots and Systems (IROS)*, pp. 5459–5466.
- [5] F. Roscia, A. Cumerlotti, A. Del Prete, C. Semini, and M. Focchi, "Orientation control system: Enhancing aerial maneuvers for quadruped robots," *Sensors*, vol. 23, no. 3, 2023. [Online]. Available: <https://www.mdpi.com/1424-8220/23/3/1234>
- [6] G. Wenger, A. De, and D. E. Koditschek, "Frontal plane stabilization and hopping with a 2dof tail," in *2016 IEEE/RSJ International Conference on Intelligent Robots and Systems (IROS)*, pp. 567–573.
- [7] X. Chu, C. H. D. Lo, C. Ma, and K. W. S. Au, "Null-space-avoidance-based orientation control framework for underactuated, tail-inspired robotic systems in flight phase," *IEEE Robotics and Automation Letters*, vol. 4, no. 4, pp. 3916–3923.
- [8] Y. Tang, J. An, X. Chu, S. Wang, C. Y. Wong, and K. Au, "Towards safe landing of falling quadruped robots using a 3-dof morphable inertial tail," *arXiv preprint arXiv:2209.15337*, 2022.
- [9] V. Kurtz, H. Li, P. M. Wensing, and H. Lin, "Mini cheetah, the falling cat: A case study in machine learning and trajectory optimization for robot acrobatics," in *2022 International Conference on Robotics and Automation (ICRA)*, pp. 4635–4641.
- [10] B. Katz, J. D. Carlo, and S. Kim, "Mini cheetah: A platform for pushing the limits of dynamic quadruped control," in *2019 International Conference on Robotics and Automation (ICRA)*, 2019, pp. 6295–6301.
- [11] Q. Nguyen, M. J. Powell, B. Katz, J. Di Carlo, and S. Kim, "Optimized jumping on the mit cheetah 3 robot," in *2019 International Conference on Robotics and Automation (ICRA)*, pp. 7448–7454.
- [12] C. Nguyen and Q. Nguyen, "Contact-timing and trajectory optimization for 3d jumping on quadruped robots," in *2022 IEEE/RSJ International Conference on Intelligent Robots and Systems (IROS)*, pp. 11994–11999.
- [13] M. Chignoli and S. Kim, "Online trajectory optimization for dynamic aerial motions of a quadruped robot," in *2021 IEEE International Conference on Robotics and Automation (ICRA)*, pp. 7693–7699.
- [14] M. Chignoli and P. M. Wensing, "Variational-based optimal control of underactuated balancing for dynamic quadrupeds," *IEEE Access*, vol. 8, pp. 49785–49797.
- [15] N. Rudin, H. Kolvenbach, V. Tsounis, and M. Hutter, "Cat-like jumping and landing of legged robots in low gravity using deep reinforcement learning," *IEEE Transactions on Robotics*, vol. 38, pp. 317–328.
- [16] J. Qi, H. Gao, H. Yu, M. Huo, W. Feng, and Z. Deng, "Integrated attitude and landing control for quadruped robots in asteroid landing mission scenarios using reinforcement learning," *Acta Astronautica*, 2022.
- [17] G. Bledt, "Regularized predictive control framework for robust dynamic legged locomotion," Ph.D. dissertation, Massachusetts Institute of Technology, 2020.
- [18] Y. L. Jingwen Zhang, Junjie Shen and D. Hong, "Design of a jumping control framework with heuristic landing for bipedal robots," <https://arxiv.org/pdf/2304.00536.pdf>, 2023.
- [19] S. H. Jeon, S. Kim, and D. Kim, "Online optimal landing control of the mit mini cheetah," in *International Conference on Robotics and Automation (ICRA)*, pp. 178–184.
- [20] M. H. Raibert, *Legged robots that balance*. MIT press, 1986.
- [21] R. Blickhan, "The spring-mass model for running and hopping," *Journal of biomechanics*, vol. 22, no. 11-12, pp. 1217–1227, 1989.
- [22] X. Xiong and A. D. Ames, "Bipedal hopping: Reduced-order model embedding via optimization-based control," in *2018 IEEE/RSJ International Conference on Intelligent Robots and Systems (IROS)*, 2018, pp. 3821–3828.
- [23] P.-B. Wieber, R. Tedrake, and S. Kuindersma, "Modeling and control of legged robots," in *Springer handbook of robotics*. Springer, 2016, pp. 1203–1234.
- [24] S. Kajita and K. Tani, "Study of dynamic biped locomotion on rugged terrain-derivation and application of the linear inverted pendulum mode," in *Proceedings. 1991 IEEE International Conference on Robotics and Automation (ICRA)*, pp. 1405–1406.
- [25] J. E. Pratt and S. V. Drakunov, "Derivation and application of a conserved orbital energy for the inverted pendulum bipedal walking model," in *Proceedings 2007 IEEE International Conference on Robotics and Automation (ICRA)*, pp. 4653–4660.
- [26] J. Pratt, J. Carff, S. Drakunov, and A. Goswami, "Capture point: A step toward humanoid push recovery," in *2006 6th IEEE-RAS international conference on humanoid robots*, pp. 200–207.
- [27] V. Barasuol, J. Buchli, C. Semini, M. Frigerio, E. R. De Pieri, and D. G. Caldwell, "A reactive controller framework for quadrupedal locomotion on challenging terrain," in *2013 IEEE International Conference on Robotics and Automation (ICRA)*, pp. 2554–2561.
- [28] C.-T. Chen, *Linear system theory and design*, 3rd ed. Oxford University Press, 1999, ch. 4, pp. 106 – 117.
- [29] A. Herzog, L. Righetti, F. Grimmering, P. Pastor, and S. Schaal, "Balancing experiments on a torque-controlled humanoid with hierarchical inverse dynamics," in *2014 IEEE/RSJ International Conference on Intelligent Robots and Systems (IROS)*, pp. 981–988.
- [30] M. Focchi, A. Del Prete, I. Havoutis, R. Featherstone, D. G. Caldwell, and C. Semini, "High-slope terrain locomotion for torque-controlled quadruped robots," *Autonomous Robots*, vol. 41, pp. 259–272, 2017.
- [31] Unitree. Go1 - accompany you to the world. [Online]. Available: <https://www.unitree.com/en/go1/>
- [32] M. Focchi, F. Roscia, and C. Semini, "Locosim: an open-source cross-platform robotics framework," *arXiv preprint arXiv:2305.02107*, 2023.
- [33] J. Carpentier, G. Saurel, G. Buondonno, J. Mirabel, F. Lamiraux, O. Stasse, and N. Mansard, "The pinocchio c++ library: A fast and flexible implementation of rigid body dynamics algorithms and their analytical derivatives," in *2019 IEEE/SICE International Symposium on System Integration (SII)*, pp. 614–619.